S-Parameter Sampling in the Frequency Domain and Its Time-Domain Response

Aldo Morales, *Senior Member, IEEE*, Sedig S. Agili, *Senior Member, IEEE*, and Taoufik Meklachi

***Abstract*— S-parameter characterization of high-speed interconnect components is prone to numerical, modeling, and/or measurement error due, in part, to the sampled nature of the data. This is a problem in modern package design where extensive signal integrity simulations are required to validate a system's performance. This article presents a new method of treating sampled S-parameter data where a criterion is developed to clearly state the minimum number of S-parameter frequency points required to adequately represent an analog physical system in the frequency domain. This criterion is akin to the Nyquist principle when sampling in the time domain. Based on this principle, the proper time-domain representation of S-parameters can be obtained using the inverse fast Fourier transform (IFFT). However, in order to use the IFFT, the bilinear transformation is applied to the vector fit S-parameters to place them in the z-domain. From the z-domain, the proper discrete impulse response is obtained. A lower bound, based on the discrete Heisenberg principle, is also offered to deal with frequency–time resolution of the S-parameters. The proposed method is successfully tested in the measured and simulated S-parameter data. The usefulness of this method is to accurately represent the time-domain behavior of the physical system S-parameter data, i.e., time delay causality, and, therefore, facilitates the applications of well-developed digital signal processing (DSP) techniques in S-parameter sampled data.**

***Index Terms*— Bilinear transformation, frequency domain Nyquist rate, Heisenberg principle, inverse fast Fourier transform (IFFT), S-parameters, time delay causal.**

I. Introduction

SIMULATION of modern high-speed interconnects involves the cascade of behavioral models from the transmitter to the receiver. These models are typically represented in terms of tabulated S-parameters or macromodels that are established by full-wave modeling or measurement. However, these techniques are prone to numerical, modeling, and measurement errors that can lead to nonphysical behavior, such as passive structures producing gain [1]–[9] or the system being noncausal [10]–[22]. For example, in simulations [10], it was pointed out that if the Hilbert transform is not maintained between the real and imaginary parts of the complex permittivity, then causal problems will arise. This is a serious problem in signal integrity analysis because nonpassive/noncausal elements can cause an entire structure to become unstable resulting in failed simulations or lack of convergence. These problems are compounded by the fact that the initial acquisition of an S-parameter behavior model can be time-consuming, and repeating such a process does not guarantee that the additional attempt will be passive/causal. For these reasons, research in developing methods for testing nonphysical behavior of the S-parameter data has gained interest.

For example, a nonphysical behavior, such as causality in S-parameters, has been studied under different approaches [11]–[14]. In these articles, methods to restore causality based on a modified Hilbert transform or most recently using a minimum phase filter [12] have been discussed. Other articles present causality check and restoration based on polynomial periodic continuations [15], [16]. However, as discussed in [11]–[16], most of the algorithms use sampled data and interpolate between the sampled points utilizing either Lagrange interpolators or cubic splines, i.e., assuming some continuity between the sampled points. As will be demonstrated in this article, without considering the constraints of sampling in the frequency domain, the abovementioned methods will be subject to false positives or false negatives. Examples of this behavior will be provided.

Several articles [23]–[26] have demonstrated the use of the FFT in obtaining S-parameters from time-domain measurements. Particularly, in a seminal article [23], several sources of error were investigated, including aliasing, truncation, and noise. Aliasing, of course, occurs when the Nyquist frequency is not high enough such that it introduces error on the obtained S-parameter data. In this article, in a similar fashion, obtaining the time-domain data from S-parameter is pursued, where a newly time-domain Nyquist rate is obtained, indicating the minimum number of frequency points that the sampled S-parameter data must contain in order to obtain its true time-domain physical behavior. To demonstrate this concept, we start with an impulse response of a basic delay line. Then, its transfer function (TF) [23] is obtained and sampled in the frequency domain. The analysis of the sampled TF allows us to derive the Nyquist rate that is twice the time delay of the transmission line (TL). In fact, this is dual to the traditional Nyquist rate [27] where the minimum sampling frequency is greater than twice the maximum frequency of

Manuscript received May 29, 2020; accepted August 21, 2020. Date of publication September 8, 2020; date of current version December 1, 2020. The Associate Editor coordinating the review process was Dr. Guglielmo Frigo. *(Corresponding author: Aldo Morales.)*

Aldo Morales and Sedig S. Agili are with the Electrical Engineering Program, Penn State Harrisburg, Middletown, PA 17057 USA (e-mail: awm2@psu.edu; ssa10@psu.edu).

Taoufik Meklachi is with the Mathematics Program, Penn State Harrisburg, Middletown, PA 17057 USA (e-mail: txm98@psu.edu).

Digital Object Identifier 10.1109/TIM.2020.3022440

the baseband signal. In other words, before obtaining the number of frequency points of the S-parameters, the time delay characteristic of the device under test (DUT) needs to be estimated (or measured). This Nyquist rate is then generalized to any analog real system. Furthermore, the well-known final and initial value Theorems are used to ensure the time-boundedness of the S-parameter data, i.e., their impulse response is time-limited, and hence, its energy is bounded. In addition, the time boundedness of the S-parameters indicates that this data does not need to be obtained up to infinite frequency, which is practically impossible. However, through the dual sampling theorem, the time-domain behavior of an analog system can be approximated from its S-parameter data to any level of accuracy [28].

Since, in many articles [10], [12], [13], [18]–[22], the inverse fast Fourier transform (IFFT) on the S-parameter data is directly applied to obtain the impulse response, we pointed out that this is not the correct approach since the S-parameter data are a sampled representation of an analog system not of a digital system. The fact that both the transform and the FFT work with complex numbers, which does not mean that we arbitrarily can take the IFFT of the S-parameter sampled data. The IFFT works on the unit circle while the Fourier transform works on the imaginary line [27]. Therefore, there is a big difference between the two. In order to appropriately find the impulse response from the S-parameter, a bilinear transformation of the S-parameter data is needed via vector fitting (VF) of the data [17], [29]–[36]. For example, in [17], a modified bilinear transformation was proposed to bridge the gap between the analog and sampled S-parameter data, but it was not used extensively.

After VF and bilinear transformation, all the data are placed in the discrete frequency domain; one can then take the IFFT to obtain the corresponding time-domain impulse response. Note that after the VF is obtained, the impulse response can be derived by using the inverse Laplace transform but is cumbersome to do. In cases where the VF does not fit the S-parameter data, such as with noncausal data, one approach is to allow the VF to place poles on the right side of the s-plane [13]. This method will make the system causal but unstable. One better approach is to iteratively calculate the advance as in [22] but using the bilinear transformation as proposed here and then use the IFFT. Once the proper advance is obtained, one can apply a corresponding delay to cancel the advance since all real physical systems must be causal. However, VF cannot be used without complying with the proposed Nyquist rate condition mentioned earlier; otherwise, the time representation is not the true impulse response of the DUT. Note that since obtaining this impulse response from S-parameters, in essence also involves time–frequency resolution, a discrete lower bound version of the Heisenberg principle [37] is provided in this article.

This article is organized as follows. In Section II, a new Nyquist rate for S-parameters is presented to accurately represent an ideal TL. In Section III, this rate is found for general cases. In Section IV, a discrete Hilbert transform, time sampling theorem, and time–frequency resolution issues of the S-parameters are discussed. In addition, a time–frequency bound is offered based on the discrete Heisenberg principle. The proposed method is applied to the measured and simulated S-parameter data. Results are presented in Section V. Conclusions are given in Section VI.

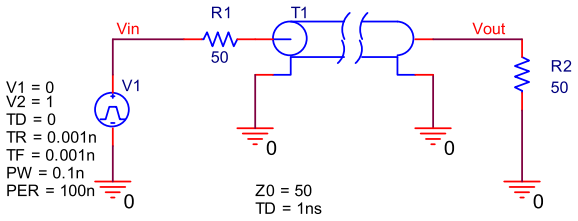

Fig. 1. Ideal TL setup.

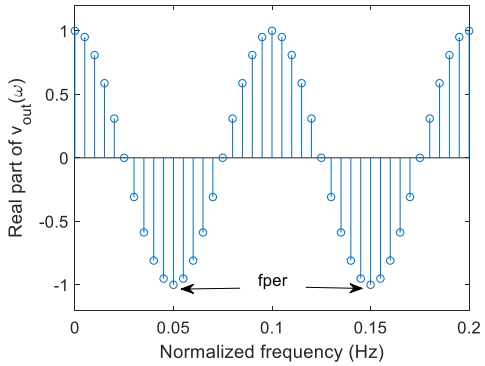

Fig. 2. Sampling of the real part of (7), showing up to 0.2 normalized Hz.

II. Basic Principles

In this section, some basic principles are reviewed. Starting the analysis with a simple but illustrative example of an ideal TL properly matched at both ends, as shown in Fig. 1. This TL has an impulse response of a delay

$$h(t) = \delta(t - t_{\max}) \tag{1}$$

where $t_{\max}$ is the TL time delay.

The TF of this ideal TL is [23]

$$H(\omega) = e^{-j\omega t_{\max}} = \cos(\omega t_{\max}) - j\sin(\omega t_{\max}) \tag{2}$$

where $\cos(\omega t_{\max})$ and $-j\sin(\omega t_{\max})$ are the Hilbert transform [38] of each other even though $H(\omega)$ is not square-integrable, as in

$$H_R(\omega) = \frac{1}{\pi} P \int_{-\infty}^{\infty} \frac{H_I(\omega')}{\omega - \omega'} d\omega' \quad \text{(a)}$$
$$H_I(\omega) = -\frac{1}{\pi} P \int_{-\infty}^{\infty} \frac{H_R(\omega')}{\omega - \omega'} d\omega \quad \text{(b)} \tag{3}$$

where $H_R(\omega)$ and $H_I(\omega)$ are the real and imaginary parts of $H(\omega)$, respectively, and P denotes the principal value. Note that $H(\omega)$ needs to be known up to an infinite frequency span for (3) to hold. However, since (2) represents a power signal in the frequency domain [39], one can readily use the discrete Hilbert transform [27], without needing infinite frequency. We also note that, for a well-matched network, such as the

one in Fig. 1, the relationship between the TF and its S_{21}-parameters is given by [18]

$$H(\omega) = \frac{S_{21}(\omega)}{2}. \tag{4}$$

The S-parameter representation of the simple TL of Fig. 1 can be obtained experimentally (or in a simulation) when the TL is excited with a "train of sinusoids" that is launched at its input (with proper terminations). Without loss of generality and by convenience, let us assume that the TL input voltage is described by the following sum:

$$v_{in}(t) = \sum_{i=0}^{\max} 2 \times \cos(\omega_i t). \tag{5}$$

The output voltage is described as the following convolution:

$$v_{\text{out}}(t) = \left(\sum_{i=0}^{\max} \cos(\omega_i t) \right) * \delta(t - t_{\max}). \tag{6}$$

Using standard techniques, in the frequency domain, the representation is given by the following equation:

$$\begin{aligned} V_{\text{out}}(\omega) &= \left(\sum_{i=0}^{\max} (\pi\,\delta(\omega + \omega_i) + \pi\,\delta(\omega - \omega_i)) \right) \\ &\quad \times (\cos(\omega t_{\max}) - j\,\sin(\omega t_{\max})) \\ &= \pi \sum_{i=0}^{\max} \underbrace{[\cos(\omega_i t_{\max}) + j\,\sin(\omega_i t_{\max})]}_{\text{Negative frequency}} \\ &\quad + \underbrace{[\cos(\omega_i t_{\max}) - j\,\sin(\omega_i t_{\max})]}_{\text{Positive frequency}}. \end{aligned} \tag{7}$$

It is apparent that the train of cosine forces sampling in the frequency domain of $H(\omega)$. An example of the real part, normalized to π, of (7) is shown in Fig. 2. We also note that, in practice (or simulation), only the positive frequency of (7) is obtained.

In Fig. 2, the separation between two the frequency samples (sample interval) is f_i, and f_{per} is the distance between the two equal peaks in the frequency domain. In order to properly sample the real (imaginary) part of the abovementioned frequency response (7), it is evident that

$$2 f_i < f_{\text{per}}. \tag{8}$$

Note that $t_{\max}$ is fixed, and then, $f_{\text{per}} = 1/t_{\max}$; let $t_i = 1/f_i$, and hence, using (8), we now have the frequency equivalent (dual) theorem of sampling in the time domain

$$t_i > 2 \times t_{\max} \tag{9}$$

i.e., in order to fully recover the time-domain signal, the sampling in the frequency domain should be fine enough to meet (9). In other words, if (9) is not satisfied, then "time aliasing" will occur.

Note that if (9) is met, then the TF $H(\omega)$ of (2) is equivalent to its TF in the z-domain as follows:

$$\begin{aligned} H(z) &= z^{-n_{\max}}|_{z=e^{j\Omega}}, \quad \Omega = \frac{2\pi f}{f_s} \\ H(e^{j\Omega}) &= e^{-j2\pi f T_s n_{\max}} \end{aligned} \tag{10}$$

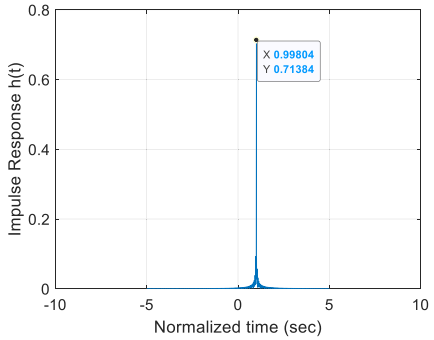

Fig. 3. IFTT of the TL.

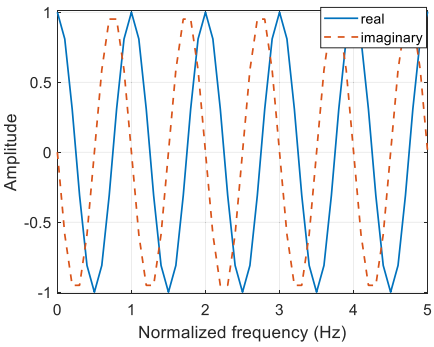

Fig. 4. Real and imaginary parts of the analytical signal of (5).

and, for convenience, set $t_{\max} = n_{\max} T_s$. Note that f_s and T_s [T_s is implicit in (10)] are the sampling frequency and sampling period, respectively, where $f_s = 2 \times f_{\max}$; Ω is the discrete frequency. Equation (10) is valid since the delta function is essentially the same in both the discrete and analog frequency domains. Hence, the IFFT can be used. It is important to note if (9) is not met, the impulse response obtained via the IFFT is not correct and does not represent the true impulse response. To demonstrate these concepts, assume that the S-parameters data of the TL are taken with frequency sample interval $f_i = 0.1$ GHz and $f_{\max} = 40$ GHz; therefore, $t_i = 10$ ns with $t_{\max} = 1$ ns, and this represents an oversampled case. Using a normalized amplitude of 1 V, the IFFT of (7) is obtained and shown in Fig. 3. The impulse response of the system shows that the system is causal and matches (1) at normalized 1 s. This agrees with the metric proposed in [40], which defines that system must be not only causal in the pure sense, i.e., no output should appear before $t = 0$, but also delay causal. The delay causality property of a system means that signal should not appear at the output before its intrinsic time delay [40].

For completeness, the real and imaginary parts of the output voltage of (7) and Fig. 3 are shown in Fig. 4. As it is apparent, it follows the Hilbert transform of (2) and (3).

To compare the time behavior of the abovementioned analytical signal (9) to a well-known, Lagrange-based causality algorithm [13], its error bound is shown in Fig. 5, and it depicts that it passes the causality check. However, the algorithm does not show if the system is delay causal [40].

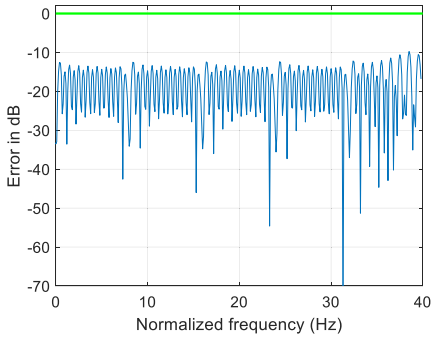

Fig. 5. Error bound from [13] showing that the frequency response passes the causality check.

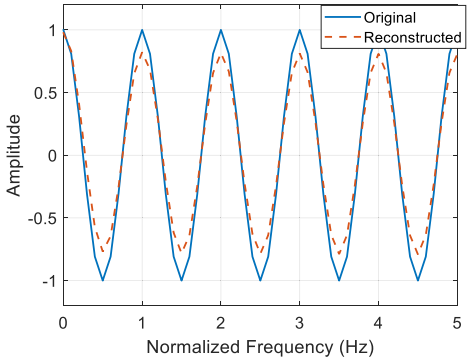

Fig. 6. Real part of the reconstructed S-parameter using [13].

For comparison purposes, we show the real part of the input (7) of the abovementioned system to the reconstructed real part of the Langrage-based method, as shown in Fig. 6. One can see that the difference between the input signal and the reconstructed signal [13] is small, resulting in a small error bound, as shown in Fig. 5.

For the case when $f_i = 0.4545$ GHz and $f_{\max} = 100$ GHz, now $t_i = 2.2$ ns, and again $t_{\max} = 1$ ns, i.e., barely over the limit of (9), the IFFT of the new frequency response, via (10), is shown in Fig. 7.

Fig. 7 shows that the system has the correct system delay of 1 s (normalized) properly identified (minus Gibbs effect). Again, the real and imaginary parts of (7) are shown in Fig. 8. Notice that the frequency response has sharp transitions due to barely sampling over the limit imposed by (9).

For comparison purposes, the error bound using the Lagrange interpolator [13] is shown in Fig. 9, where the depicted error bound completely fails, i.e., provides a false negative, indicating that the system is not physical. The cause of this is that, as seen in Fig. 8, the imaginary and the real parts do not follow a Hilbert trend see (3), as shown from 2 to 6 Hz.

Furthermore, for the case when $f_i = 3.01$ GHz, a very high $f_{\max} = 600$ GHz, then $t_i = 0.332$ ns, and with $t_{\max} = 1$ ns, this is a severely undersampled case. The IFFT shows that the impulse response does not represent the TL's true behavior since its delay is close to zero, as shown in Fig. 10. Therefore, this result indicates that the signal reached the output in 0.003 ns when in fact it should take 1 ns. In other words, this result tells us that the signal reached the output 0.997 ns ahead (advance) of its supposed system delay, a clear delay system causality violation [40].

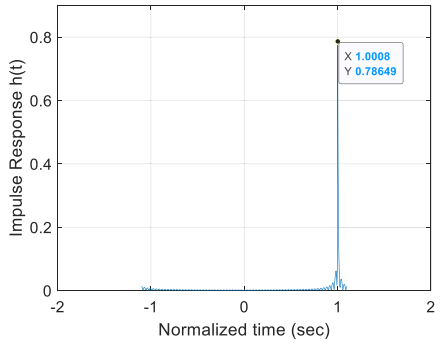

Fig. 7. IFFT when $t_i = 2.2$ ns.

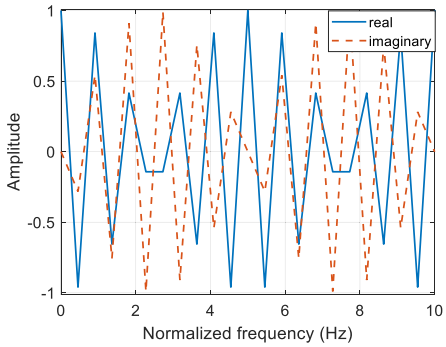

Fig. 8. Frequency response with a sampling barely over the criterion of (9).

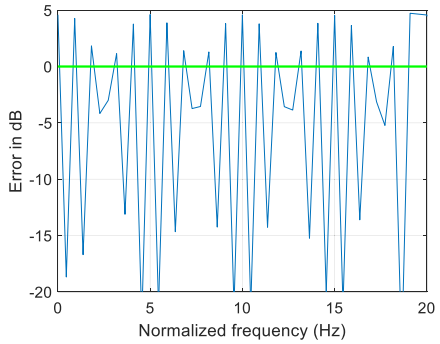

Fig. 9. False-negative.

The analytical signal for the undersampled case is shown below in Fig. 11. In this instance, the Lagrange-based method indicates that the system is causal (see Fig. 12); however, it does not provide the proper time delay representing the true physical system. Furthermore, we emphasize that this TL (or any other physical system) has a time delay; it should be not only causal but also delay causal system [40]. One can observe that the reason for this result [13] is that the undersampled analytical signal follows the Hilbert trend as in (3) [38], i.e., the real part of the analytical signal is the Hilbert transform of its imaginary part.

There are two drawbacks with checking the time behavior from frequency domain sample data, when not using (9).

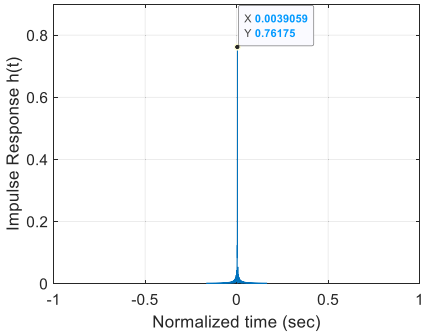

Fig. 10. Undersampled of (7) showing the nontrue time behavior of the TL system.

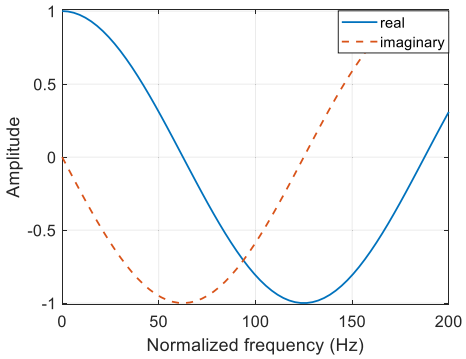

Fig. 11. Under sampled analytical signal showing the Hilbert trend.

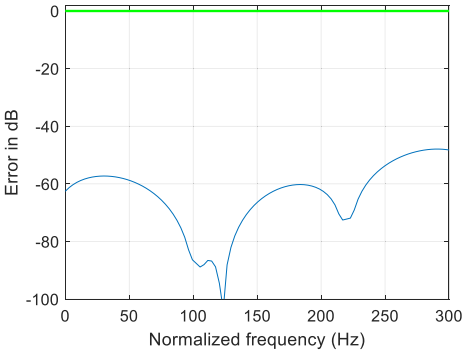

Fig. 12. Error bound is low indicating the system is causal.

For example, any interpolator-based method fails when (9) is not verified. The other is that there is no need to consider up to infinite frequency, as in the abovementioned examples, since the limit imposed by (9) is enough to recover the impulse response. The impulse response can be recovered with any level of accuracy if (9) is met [28]. Of course, in the IFFT method, the Gibbs effect needs to be considered.

III. General Cases

Section II sets the stage for more general cases, which will be presented in this section. In a general case, a DUT needs to be characterized by its TF in the Laplace domain. Without loss of generality, assume that S_{21} behaves like a low-pass filter and can be represented by

$$S_{21}(s) = H_{\mathrm{LP}}(s) = \frac{s^n + a_{n-1}s^{n-1} + \ldots a_2 s^2 + a_1 s + a_0}{s^m + b_{m-1}s^{m-1} + \ldots b_2 s^2 + b_1 s + b_0} \tag{11}$$

where $n < m$ and $s = j\omega$. We note that (11) is of order $O(1/\omega)$, i.e., decreases as $\omega \to \infty$[38]. Note also that the scale factor in (4) is ignored in (11). It is also well understood that S_{21} and S_{11} have the following constraint for passivity (without considering losses):

$$|S_{21}(\omega)|^2 + |S_{11}(\omega)|^2 = 1. \tag{12}$$

Comparing the abovementioned equation with standard filter banks

$$|H_{\mathrm{LP}}(\omega)|^2 + |H_{\mathrm{HP}}(\omega)|^2 = 1. \tag{13}$$

If S_{21} is considered a low pass, then S_{11} should be a high pass and can be modeled as

$$S_{11}(s) = H_{\mathrm{HP}}(s) = \frac{s^m + c_{m-1}s^{m-1} + \ldots c_2 s^2 + c_1 s + c_0}{s^m + b_{m-1}s^{m-1} + \ldots b_2 s^2 + b_1 s + b_0}. \tag{14}$$

Since passive systems are bounded-input–bounded-output (BIBO) systems, both numerator and denominator of (14) must have the same order, implying that (14) is of an order $O(1)$ [38], i.e., will be constant as $\omega \to \infty$. In addition, because of the restriction imposed by the passivity condition, it can be shown that both denominators in (11) and (14) will be the same.

To obtain the TFs (11) and (14), the VF algorithm is used. VF was first proposed in [29] and has been extensively used in the signal integrity realm [30]–[36]. S-parameter data can be fit with a rational function as

$$H(s) = \sum_{k=1}^{n} \frac{d_k}{s - e_k} + c + sh \tag{15}$$

where d_k and e_k come in complex conjugate pairs, and c and h are real constants. The constant h is considered to be zero for S-parameter modeling [36] since passive systems are BIBO. The VF is a very good interpolator, and it can be tailored to a targeted fitting error. For example, it was reported that the S-parameters of a two-port dispersive multipole microstrip was vector fit with an error below −64 dB over the 0.1–30 GHz range, i.e., within a noise level of a vector network analyzer [33]. Using VF, (11) and (14) can be represented as partial fraction expansion

$$\begin{cases} S_{21} = \dfrac{d_1}{s - e_1} + \dfrac{d_2}{s - e_2} + \dfrac{d_3}{s - e_3} \cdots & \text{(a)} \\ S_{11} = c + \dfrac{g_1}{s - e_1} + \dfrac{g_2}{s - e_2} + \dfrac{g_3}{s - e_3} \cdots & \text{(b).} \end{cases} \tag{16}$$

Note that if the poles in (16) are complex, then they should come in pairs, and in general, $d_i's \neq g_i's$. Constraints can be applied to (16) by using final and initial value theorems [19], which results in

$$\begin{cases} \lim\limits_{s\to 0} sS_{21}(\omega) = \lim\limits_{t\to\infty} h_{21}(t) = 0 & \text{(a)} \\ \lim\limits_{s\to 0} sS_{11}(\omega) = \lim\limits_{t\to\infty} h_{11}(t) = 0 & \text{(b).} \end{cases} \tag{17}$$

where $h_{21}(t)$ and $h_{11}(t)$ are the continuous-time inverse Fourier transform of S_{21} and S_{11}, respectively. Note that (17) indeed guarantees that the impulses response $h_{21}(t)$ and $h_{11}(t)$ are time-limited even though they are not known. Consequently, they have finite energy in the frequency domain as per Parseval's theorem. This fact implies that one can impose a time sampling constraint as in (9) to properly sample the S-parameter in the frequency domain. For completeness, using the initial value theorem in (16) gives

$$\begin{cases} \lim_{s\to\infty} sS_{21}(\omega) = \lim_{t\to 0} h_{21}(t) = \sum_{k=1}^{n} d_k & \text{(a)} \\ sS_{11}(\omega)\lim s \to \infty = \lim_{t\to 0} h_{11}(t) = \sum_{k=1}^{n} g_k + c\delta(t) & \text{(b).} \end{cases} \tag{18}$$

Additional constraints can be imposed on (18) as

$$\begin{cases} \lim_{t\to 0} h_{21}(t) = \sum_{k=1}^{N} d_k = 0 & \text{(a)} \\ \lim_{t\to 0} h_{11}(t) = -c\delta(t) & \text{(b).} \end{cases} \tag{19}$$

Note that (19a) is valid since no response should arrive at port 2 at time 0, as per the delay causal system [40]. In addition, (19b) indicates that, at $\omega = \infty$, all the energy would be reflected back at port 1 if no losses are considered, hence the negative sign.

After ensuring time-boundness with (17) and following a similar procedure in Section II, the impulse train (i.e., the FT of the cosine sequence) multiplies the TF (16a), or (11), of the DUT as

$$\begin{aligned} V_{21}(\omega) &= \left(\pi \sum_{i=0}^{\max} (\delta(\omega+\omega_i) + \delta(\omega-\omega_i))\right) \times (S_{21}(\omega)) \\ &= \sum_{i=-\max}^{\max} S_{21}(\omega_i) \\ &= S_{21}(\omega)|_{s=j\omega_i}, \quad i = -\max, \ldots, -1, 0, 1, \ldots, \max \\ &= \sum_{k=0}^{n} \frac{d_k}{s-e_k}\bigg|_{s=j\omega_i} \\ &\qquad i = -\max, \ldots, -1, 0, 1, \ldots, \max \end{aligned} \tag{20}$$

where, for simplicity, (20) has been normalized with respect to π, as well as taken into account the positive- and negative-frequency components of the output voltage as in (7). Equation (20) also needs to comply with (9) in order to fully recover the impulse response.

The above sampled data S_{21} (or S_{11}) of (20) is provided in tabular form, but we stress that it is a tabulated data of a continuous analog system. We note that most authors mistakenly take the IFFT of the above data, without realizing that the IFFT is used for systems that are discrete to begin with. The IFFT works in the unit circle, while the Fourier transform works in the imaginary line. We again highlight that the example in Section II is unique in the sense that the TL TF in the s-domain matches its TF in the z-domain, which is not the case in general.

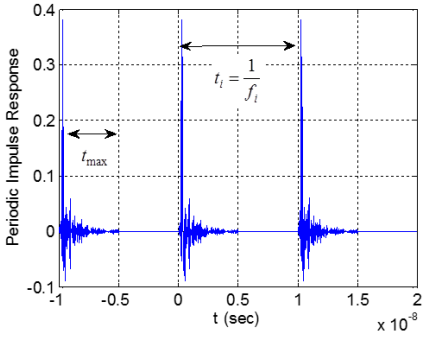

Fig. 13. Periodic impulse response.

The obtained sampled TF of (20) is bilinear transformed [27] into the z-domain as

$$S_{21}(z) = \sum_{k=1}^{n} \frac{d_k}{s-e_k}\bigg|_{s=\frac{2}{T_s}\left(\frac{z-1}{z+1}\right)} \tag{21}$$

where $T_s = 1/2f_{\max}$, $f_s = 2 \times f_{\max}$, f_s is the sampling frequency, and $f_{\max}$ is the maximum frequency of measurement or simulation. Using simple manipulation, (21) simplifies to

$$S_{21}(z) = \sum_{k=1}^{n} \frac{d_k T_s(z+1)}{z(2-e_k T_s)) - (2+e_k T_s)}. \tag{22}$$

In this transformation, poles in the left-half-plane in the s-domain are mapped inside the unit circle in the z-domain. The by-product of this bilinear transformation is that data at infinity are not required. Only data at $f_{\max}$ are needed.

Now that z-domain representation of the S_{21} sampled data is accomplished, then, one can use, without any restriction, the IFFT on the obtained z-domain representation of (22). This results in a periodic impulse response as [17], [27], [41]

$$h_{21P}(t) = \frac{1}{f_i} \sum_{n=-\infty}^{\infty} h_{21}(t - nt_i). \tag{23}$$

A truncated plot of (23) is shown in Fig. 13, where, in the figure, $t_i = 1/f_i$. Note that due to the nature of the IFFT, $h_{21P}(t)$ is periodic and discrete [17], [27], [41], [42], where the period between consecutive impulse responses is t_i as indicated in Fig. 13. Following the development in (9) and as evident in Fig. 13, to avoid time aliasing, we need

$$t_i > 2 \times t_{\max} \tag{24}$$

where $t_{\max}$ is now defined as the maximum length of the system's impulse response, which is guaranteed by the final value theorem (17).

Note again that t_i in (24) is related to the frequency separation between S-parameter data points f_i. Therefore, decreasing the separation between frequency points increases t_i and, hence, decreases the likelihood of having time aliasing problems. The question now is how to obtain $t_{\max}$ since we do not have this information in the S-parameters data. There are different strategies for choosing a realistic $t_{\max}$. For example, one can use five times the estimated time delay t_d, i.e., propagation delay, of the DUT [41], or five times

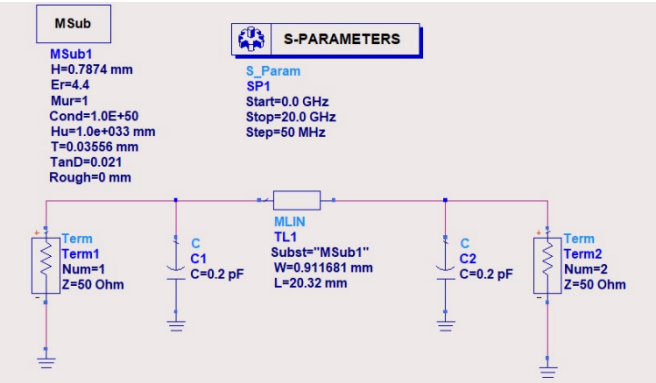

Fig. 14. Mismatched TL [49].

its maximum group delay [43], [44] to accommodate any transient behavior, such as resonant traveling waves dying out (assuming dispersive and lossy materials); therefore, a good estimate is

$$t_i > 2 \times t_{\max} = 2(5 \times t_d) = 10 \times t_d. \tag{25}$$

Note that without complying with the sampling theorem (25), the number of data points in the S-parameter will not represent the true time behavior of the system, as shown in Section II. Therefore, in order to determine the number of points needed for S-parameter measurement or simulation, first, the time delay t_d of the system from the physical dimensions and materials of the DUT is obtained; then, using the sampling theorem (25), calculate t_i, followed by f_i, and, hence, determine the total number of points to $f_{\max}$. Consequently, a designer can work with the above theorem to safely estimate the number of data points needed in the frequency, not just based on $f_{\max}$ but rather on $f_{\max}$ in conjunction with (25).

Again, we note two important issues: VF (or any interpolator) will truly represent the system if the sampled data comply with the Nyquist rate of (25); second, one can obtain the impulse response by finding the inverse Laplace transform of the VF results, but it is a cumbersome process. Instead, the bilinear transformation is utilized to place the s-domain TF in the z-domain, where one can use the IFFT to find the impulse response. Hence, in this article, the VF has been modified to work in the z-domain rather than in the s-domain. In addition, all the well-developed digital signal processing (DSP) techniques can be applied to this z-domain data, such as windowing and filtering.

In cases where the VF does not fit, such as with noncausal data, one approach is to allow the VF to place poles on the right-hand side. This method will make the system causal but unstable, i.e., not usable [13]. For example, consider S_{21} with an advance as follows:

$$S_{21}(s) = e^{j\omega\tau_1} \frac{s^n + a_{n-1}s^{n-1} + \ldots a_2 s^2 + a_1 s + a_0}{s^m + b_{m-1}s^{m-1} + \ldots b_2 s^2 + b_1 s + b_0} \tag{26}$$

where τ_1 is an advance; in this case, VF will fail. Rather than flipping poles, one better approach is to iteratively calculate the advance as in [22] but using the bilinear transformation as proposed here, not the direct IFFT. An example of this process will be illustrated in a follow-up article.

IV. Sampled S-Parameters Time–Frequency Resolution

Since data rates keep increasing to 100 Gb/s and beyond, designers need many more data points than before, which makes measurements and/or simulations more time-consuming. In Section III, an efficient rule to obtain the minimum number of points on S-parameter measurements and/or simulations was presented, which still allows obtaining reliable time-domain information from sampled frequency data. However, there is also the issue of time–frequency resolution, in other words, how finite the frequency interval needs to be and still have a good resolution in the time domain, or vice versa. Here, we offer a Heisenberg principle [17], [37], [45]–[48] to guarantee that a lower bound will not be reached and still have a discernible time–frequency resolution.

If the S-parameters were continuous, the Heisenberg uncertainty principle could be described as

$$D_o(h_{21}(t)) \times D_o(S_{21}(f)) \geq \frac{\|h_{21}(t)\|_2^4}{16\pi^2} \tag{27}$$

where

$$\begin{cases} D_0(h_{21}(t)) = \displaystyle\int_{-\infty}^{\infty} t^2 |h_{21}(t)|^2 dt & \text{(a)} \\ D_0(S_{21}(f)) = \displaystyle\int_{-\infty}^{\infty} f^2 |S_{21}(f)|^2 df & \text{(b)} \end{cases} \tag{28}$$

$\|\cdot\|$ is the norm, and $h_{21}(t)$ is the continuous inverse Fourier transform of S_{21}. Equation (27) in essence provides a bound based on the variance in the time and frequency domains, respectively. The integration in (28a) converges, since, in this case, we are dealing with time-limited (impulse response) signals, as shown by the final value theorem in (17). The frequency-domain integration (28b) is also guaranteed convergence by using Parseval's theorem. Since the frequency integral of (28b) is an even function, then

$$D_o(S_{21}(f)) = 2\int_0^{\infty} f^2 |S_{21}(f)|^2 df. \tag{29}$$

However, as seen in Section III, the sampled data obtained from the VNA or simulation has a finite span of N frequency points as in (20); then, (29) can be approximated as

$$D_0(S_{21}(f)) \cong 2\sum_{n=0}^{N-1} (nf_i)^2 |S_{21}(nf_i)|^2 f_i \tag{30}$$

where $f = nf_i$. Simplifying (30) gives

$$D_0(S_{21}(f)) \cong 2(f_i)^3 \sum_{n=0}^{N-1} (n)^2 |S_{21}(nf_i)|^2. \tag{31}$$

Noting that $S_{21}(nf_i)$ in (31) has an upper bound of 1 for passive systems and has finite energy, then (31) reduces to

$$\begin{aligned} D_0(S_{12}(f)) &\leq 2(f_i)^3 \sum_{n=0}^{N-1} (n)^2 |1|^2 \\ D_0(S_{12}(f)) &\leq 2(f_i)^3 \left(\frac{(N-1)(N)(2N-1)}{6} \right). \end{aligned} \tag{32}$$

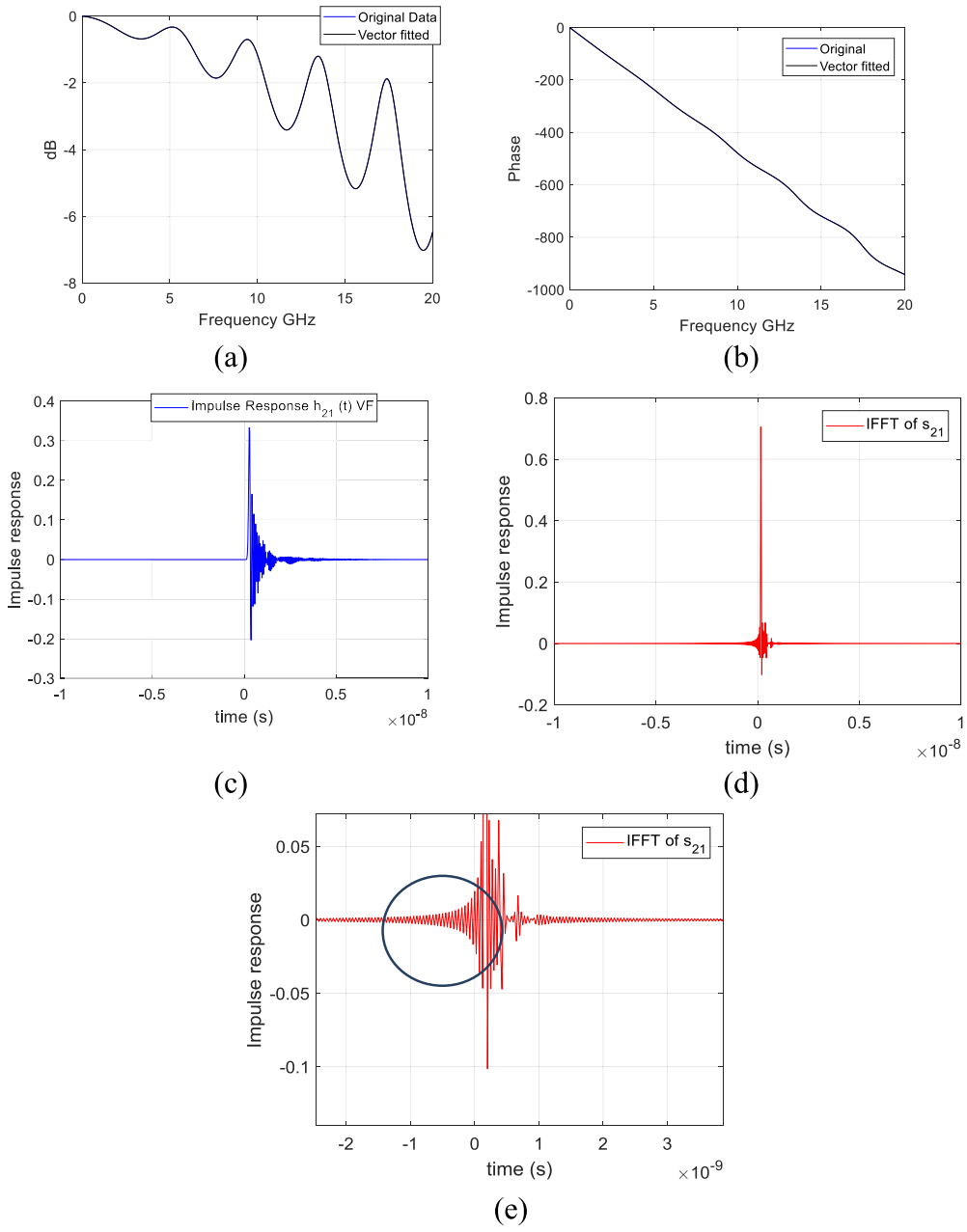

Fig. 15. (a) Magnitude S_{21}-parameters of a TL, vector fit at -81.40 dB. (b) S_{21}-parameters phase in degrees of a TL. (c) Inverse FFT of the S_{21}-parameters, after z transform. (d) Direct IFFT from sampled S_{21}-parameters. (e) Zoomed near 0 with the wrong application of the IFFT.

Typically, N is >100; then, (32) can be further simplified to

$$D_0(S_{21}(f)) \leq \frac{2(f_i)^3 N^3}{3}. \tag{33}$$

Using a similar treatment that led to (32) and (33), for the time-domain integration, with $t = nT_s$, and noting that, in (28a), there is not an even symmetry, then $D_0(h_{21}(t))$ is found to be

$$D_0(h_{21}(t)) \leq \frac{(T_s)^3 N^3}{3}. \tag{34}$$

Note that, in (33) and (34), the numbers of data points in the frequency and time domains are assumed to be the same. In addition, the norm of (27) is also modified to

$$\|h_{21}(t)\|_2^4 = \left[\left[\sum_{n=0}^{N-1} |h_{21}(nT_s)|^2\right]^{\frac{1}{2}}\right]^4 = \left[\sum_{n=0}^{N-1} |h_{21}(nT_s)|^2\right]^2 = E_t^2. \tag{35}$$

Since the problem is finding $h_{21}(nT_s)$ in (36) and the frequency data points of S_{21} are readily available, then, using Parseval's Theorem [35] in the discrete form

$$\sum_{n=0}^{N-1} |h_{21}(nT_s)|^2 = \frac{1}{N} \sum_{n=0}^{N-1} |S_{21}(nf_i)|^2. \tag{36}$$

Then

$$\sum_{n=0}^{N-1} |S_{21}(nf_i)|^2 = E \Rightarrow \sum_{n=0}^{N-1} |h_{21}(nT_s)|^2 = \frac{E}{N} = E_t. \quad (37)$$

Using (33)–(37) and simplifying, then

$$T_s^3 \times f_i^3 \geq \frac{9E_t^2}{32\pi^2 N^6}$$
$$T_s \times f_i \geq \frac{\sqrt[3]{9}E_t^{2/3}}{2(2\pi)^{2/3}N^2}. \quad (38)$$

Therefore, in this article, (38) places a new, practical lower bound on the relationship between the separation of the time samples (T_s) and the distance between frequency samples (f_i) due to the sampled nature of the S-parameters data. The constraints described in (25) and in (38) must be met in order to successfully obtain a system time delay information from passive S-parameters sampled data, therefore its true time-domain physical behavior or from time to frequency domain.

V. Examples

The abovementioned method is tested in the simulated and measured data on three different examples. The algorithm was tested first on a simple TL [49] with 50-Ω terminations and a couple of capacitors, as depicted in Fig. 14. It was simulated on ADS, with 401 frequency points, from 0 to 20 GHz. The TL length is 0.8 in (20.32 mm), with an $\varepsilon_r = 4.4$. The resulting S_{21}-parameter magnitude and phase are shown in Fig. 15(a) and (b), respectively. The S_{21}-parameter data were vector fit with an error of -81.40 dB. The vector fit of S_{21} was bilinear transformed, and then, the IFFT was taken. Fig. 15(c) shows the impulse response and indicates that the system is delay causal. This is in contrast to if the IFFT is directly applied to S_{21}-parameter sampled data [see Fig. 15(d) and (e)]. Note also that, from Fig. 15(c), one can find the system delay of approximately 0.15 ns, which agrees with the calculated time delay of $t_d = 0.145$ ns, given the length of the DUT (0.8 in), $\varepsilon_r = 4.4$, and the speed of light id 11.8 in/ns. Note that, in the abovementioned example, it was found that the algorithm complied with the time Nyquist rate (25), with an $f_{\max} =$ 20 GHz and 401 points, this corresponds to $f_i = 50$ MHz and $t_i = 20$ ns $< 10 \times t_d = 1.45$ ns, clearly an oversampled case. One can also easily verify that the Heisenberg principle bound (38) is satisfied.

The method was applied to a second DUT example, a 5-in microstrip line (see Fig. 16), with FR4 substrate. An Agilent Technologies Performance Network Analyzer (PNA) E8364B was used for S-parameter measurements. The PNA was calibrated using an electronic calibration kit N4693A, with a short-open-load-through (SOLT) calibration method, with an IF of 300 Hz. The S_{21}-parameters of the DUT magnitude and phase are shown in Fig. 17(a) and (b), respectively. The measurements were made with 1300 frequency points up to 26 GHz, and the S_{21}-parameters were back extrapolated to dc.

The measured S_{21}-paramater data were vector fit with an error of -72.99 dB and bilinear transformed to the z-domain

Fig. 16. 5-in microstrip line.

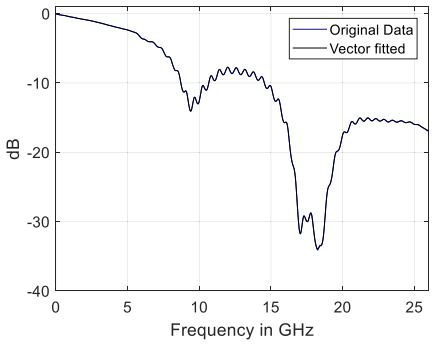

(a)

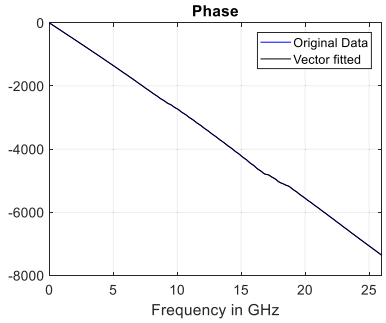

(b)

Fig. 17. (a) S_{21} magnitude for the 5-in microstrip fit with -72.99-dB error. (b) S_{21} phase, in degrees, for the 5-in microstrip.

[see Fig. 17(a) and (b)]. The IFFT of this transformation was taken, and the result is shown in Fig. 18. It depicts the proper system delay. Since this DUT is 5-in long and the number of frequency points is 1300, there is enough time for any resonant travel waves to die out. This setup was based on the 1300 points and $f_{\max} = 26$ GHz, which led to $f_i = 20$ MHz; hence, $t_i = 50$ ns. Using the speed of light of 11.8 in/ns and $\varepsilon_r = 4$, the time delay for this DUT is approximately 0.715 ns. Hence, $10 \times t_d = 7.15$ ns, which is way below t_i, another oversampled case for this measurement example.

To further verify all the postprocessing steps, a Tektronix 8200 Time Domain Reflectometer (TDR) measurement was performed on the 5-in DUT with port 2 open, and it is shown in Fig. 20. The round-trip delay is 1.44 ns, with a time delay of 0.722 ns, which is within the range of delay shown in Fig. 19 (the zoomed-in version of Fig. 18).

To illustrate how frequency undersampling affects the results in the time domain, a new measurement for this DUT was taken with 160 points, with a frequency separation of about $f_i \approx 166$ MHz, and hence, $t_i = 1/f_i = 6$ ns. The S_{21}-parameter was vector fit with -72.49-dB error. Again, the estimated time delay for this microstrip is 0.715 ns, and hence, $t_i = 6$ ns $< 10 \times t_d = 7.145$ ns; therefore,

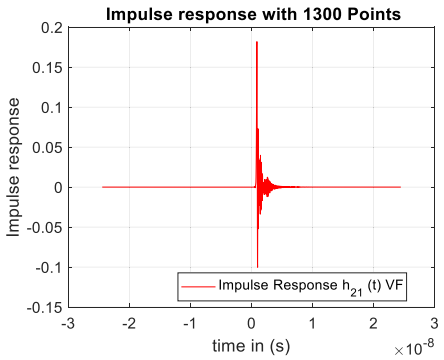

Fig. 18. Impulse response for the 5-in microstrip after bilinear transformation.

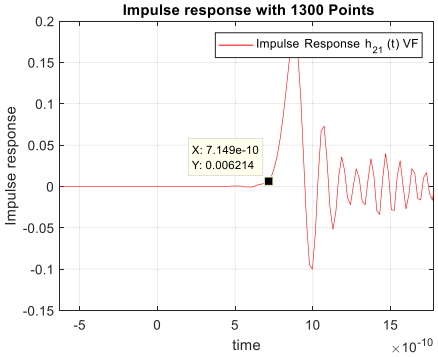

Fig. 19. Time delay of the 5-in microstrip.

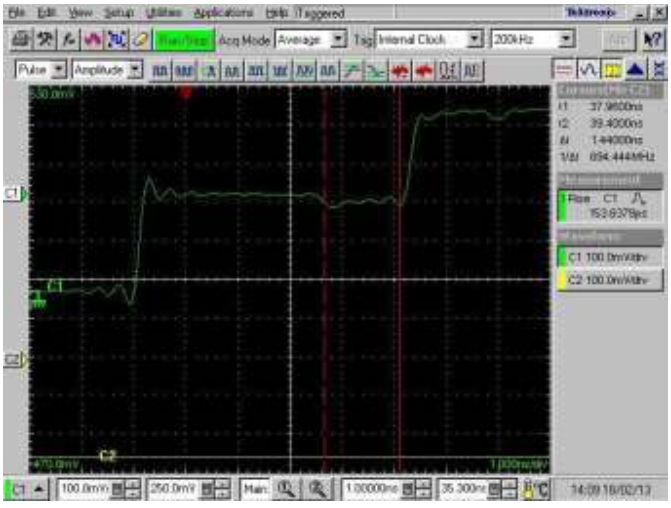

Fig. 20. TDR round trip delay of the 5-in DUT.

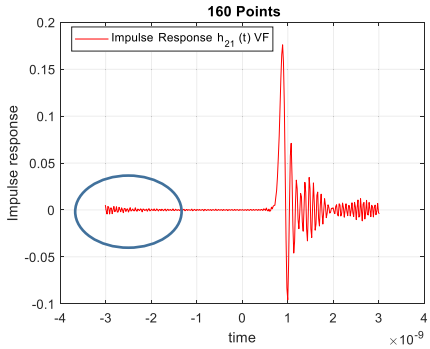

Fig. 21. Impulse response of the 5-in DUT using 160 frequency points.

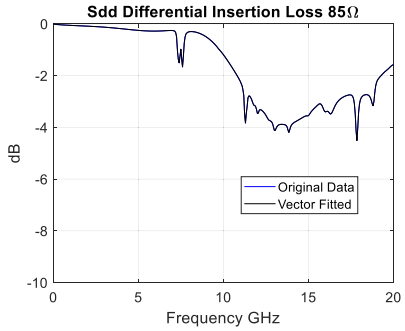

(a)

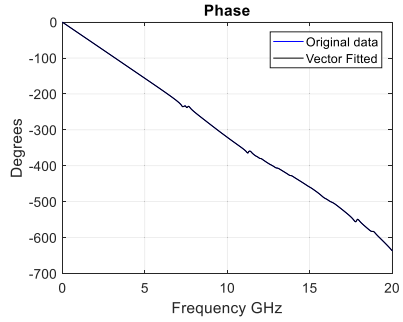

(b)

Fig. 22. (a) Insertion loss magnitude, data fit with −69.97-dB error. (b) Insertion loss phase, data fit with −69.97-dB error.

it does not meet the sampling criterion of (25). Hence, some wrapping over the negative time is shown in Fig. 21, indicating " time aliasing." Because of the undersampling in the frequency domain, it is clear, from the figure, that the time allocated (t_i) for this impulse response is not enough. This means that even with this level of VF error (−72.49 dB), there is no guarantee that the IFFT will depict the right impulse response unless (25) is verified.

If one uses the calculation based on the estimated time delay $t_d = 0.7145$ ns, and using (25), then t_i, in this case, should be greater than 7.145 ns. For instance, choosing $t_i = 8.34$ ns leads to an $f_i = 120$ MHz. Hence, for an $f_{\max}$ of 26 GHz, the minimum number of points for this example should be at least 217.

Another practical example is a PCI express Gen2 manufactured by Amphenol-FCI LLC USA, one of the companies that sponsors The Center for Signal Integrity, Penn State Harrisburg. The S-parameter data were provided, with the starting frequency of 50 MHz and the max frequency of 20 GHz with 401 points, hence having an $f_i = 64.7$ MHz. In addition, the PCIe Gen2 specifications are 85-Ω reference impedance and data rate, 5 G transfers/second (GT/s), and six differential ports. Fig. 22(a) shows the differential insertion loss for one of the differential ports, while 22(b) shows its phase.

The S_{dd21}-parameter data were vector fit with an error of −69.97 dB, bilinear transformed to z-domain, and the IFFT was taken [see Fig. 23(a) and (b)]. The figure clearly shows

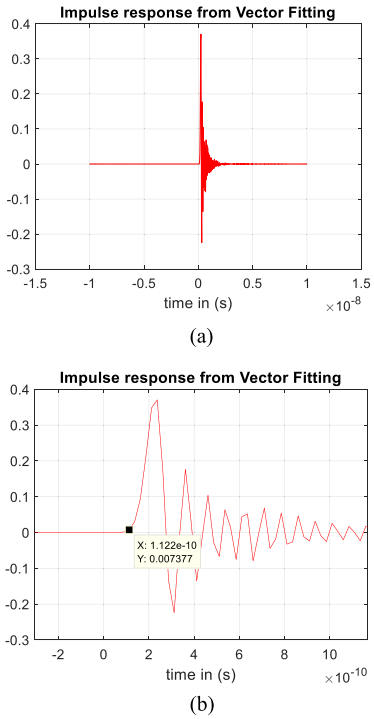

Fig. 23. (a) S_{dd21} impulse response after bilinear transformation. (b) Zoomed-in version of (a) used to back-calculate the DUT's length.

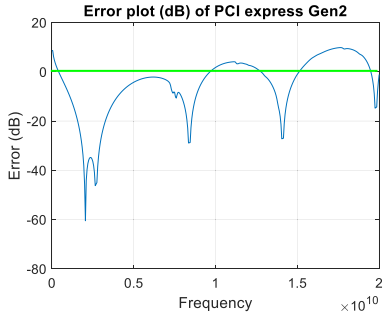

Fig. 24. Error bound using the Lagrange interpolator method [13].

the system delay of S_{dd21}. We note that this S-parameter was deemed noncausal by Amphenol-FCI using their internal tools and Keysight's Physical Layer Test System. It was also deemed noncausal by the Lagrange-based method (error above 0 dB), as shown in Fig. 24.

A zoomed-in version of Fig. 23(a) was used to back-calculate the length of this DUT [see Fig. 23(b)], with a time delay indicated in Fig. 23(b) of $t_d = 0.1122$ ns, based on $f_i = 64.7$ MHz; then, $t_i = 15.45$ ns $> 10 \times t_d = 1.122$ ns. In addition, based on the known speed of light and the dielectric value of the DUT, one can estimate its length, which is about 17 mm, within the range of the actual dimensions reported to us by Amphenol-FCI.

In all the abovementioned examples, the Heisenberg bound was checked, and in all the examples, this bound was met. The previous results are highly encouraging in accurately estimating the system time delay from sampled S-parameter data. In addition, one can easily verify the length of the DUT and apply all well-known DSP postprocessing techniques, such as windowing and filtering.

VI. Conclusion

When calculating system delay in S-parameters, most of the algorithms use IFFT from sampled S-parameter data, which is incorrect. The data provided are sampled data from an analog system, not from a digital system to which the IFFT can be readily used. In this article, the system time delay has been obtained using the well-known and well-tested algorithm, VF. Then, the bilinear transformation was utilized to move the TF from the s-domain to the z-domain. This transformation allows the IFFT to be taken. However, in order to check whether the system delay can be accurately estimated, enough data points need to be used. Hence, a comparable sampling equation has been offered similar to the Nyquist rate. The minimum separation of frequency points is found in order to avoid "time aliasing" that can lead to the wrong estimation of the system delay. Here lies one of the advantages of this method: no frequency at infinity is needed. As long as one complies with the sampling in the frequency domain, system delay can be successfully obtained. Since obtaining time information from the frequency data is an issue involving time–frequency resolution and considering that data rates continue to increase, a time–frequency bound, using the discrete version of the Heisenberg principle, was provided. The method was tested in several examples, including measured and simulated S-parameter data. Results in the tested examples demonstrate that the proposed method successfully estimated the time delay information.

Acknowledgment

The authors would like to thank Mr. Steven Smith, Amphenol LLC, for providing PCI express Gen2 data. They would also like to thank Mr. Reggie Devine, former Engineer at the Center for Signal Integrity, Penn State Harrisburg, for taking the required measurement and simulations. They would also like to thank the reviewers.

References

[1] V. Belevitch, *Classical Network Theory*. San Francisco, CA, USA: Holden-Day, 1968.

[2] Y. Wang, Z. Zhang, C.-K. Koh, G. Shi, K. H. G. Pang, and N. Wong, "Passivity enforcement for descriptor systems via matrix pencil perturbation," in *Proc. IEEE/ACM Int. Conf. Comput.-Aided Design (ICCAD)*, pp. 800–807, Nov. 2010.

[3] M. Fu, L. Xie, and H. Li, "Passivity analysis for uncertain signal processing systems," in *Proc. IEEE Int. Conf. Acoust., Speech Signal Process. (ICASSP)*, vol. 3, May 1998, pp. 12–15.

[4] S. Grivet-Talocia, "Passivity enforcement via perturbation of Hamiltonian matrices," *IEEE Trans. Circuits Syst. I, Reg. Papers*, vol. 51, no. 9, pp. 1755–1769, Sep. 2004.

[5] D. Campbell, "A simple method for restoring passivity in S-parameters using singular value decomposition," M.S. thesis, Elect. Eng. Dept., Pennsylvania State Univ., Harrisburg, PA, USA, Jun. 2009.

[6] C.-U. Lei, Y. Wang, Q. Chen, and N. Wong, "On vector fitting methods in signal/power integrity applications," in *Proc. IMECS*, Hong Kong, vol. 2, Mar. 2010, pp. 1–6. Accessed: Sep. 12, 2020. [Online]. Available: http://hub.hku.hk/bitstream/10722/129644/1/Content.pdf

[7] S. Grivet-Talocia, "An adaptive sampling technique for passivity characterization and enforcement of large interconnect macromodels," *IEEE Trans. Adv. Packag.*, vol. 30, no. 2, pp. 226–237, May 2007.

[8] B. Gustavsen and A. Semlyen, "Simulation of transmission line transients using vector fitting and modal decomposition," *IEEE Trans. Power Del.*, vol. 13, no. 2, pp. 605–614, Apr. 1998.

[9] T. D'haene and R. Pintelon, "Passivity enforcement of transfer functions," *IEEE Trans. Instrum. Meas.*, vol. 57, no. 10, pp. 2181–2187, Oct. 2008.

[10] C. Morgan, "Solutions for causal modeling and a technique for measuring, causal, broadband dielectric properties," in *Proc. DesignCon*, Santa Clara, CA, USA, 2008, pp. 1–21. Accessed: Sep. 12, 2020. [Online]. Available: https://electronicpro.com/Resource/Detail/45967

[11] P. Triverio and S. Grivet-Talocia, "A robust causality verification tool for tabulated frequency data," presented at the 10th IEEE Workshop Signal Propag. Interconnects, Berlin, Germany, May 2006.

[12] P. Triverio, "Robust causality check for sampled scattering parameters via a filtered Fourier transform," *IEEE Microw. Wireless Compon. Lett.*, vol. 24, no. 2, pp. 72–74, Feb. 2014.

[13] P. Triverio and S. Grivet-Talocia, "Robust causality characterization via generalized dispersion relations," *IEEE Trans. Adv. Packag.*, vol. 31, no. 3, pp. 579–593, Aug. 2008.

[14] P. Triverio, S. Grivet-Talocia, M. S. Nakhla, F. G. Canavero, and R. Achar, "Stability, causality, and passivity in electrical interconnect models," *IEEE Trans. Adv. Packag.*, vol. 30, no. 4, pp. 795–808, Nov. 2007.

[15] L. L. Barannyk, H. A. Aboutaleb, A. Elshabini, and F. Barlow, "Causality verification using polynomial periodic continuations for electrical interconnects," *J. Microelectron. Electron. Packag.*, vol. 11, no. 4, pp. 181–196, Oct. 2014.

[16] L. L. Barannyk, H. A. Aboutaleb, A. Elshabini, and F. D. Barlow, "Spectrally accurate causality enforcement using SVD-based Fourier continuations for high-speed digital interconnects," *IEEE Trans. Compon., Packag., Manuf. Technol.*, vol. 5, no. 7, pp. 991–1005, Jul. 2015.

[17] P. E. Dahlen, "Enhancing signal integrity design methodologies utilizing discrete frequency domain techniques," Ph.D. Dissertation, Univ. Minnesota, Minneapolis, MN, USA, Apr. 2014.

[18] J. Cho, K. Hwang, S. Jeung, and S. Ahn, "An efficient extrapolation method of band-limited S-parameters for extracting causal impulse responses," *IEEE Trans. Comput.-Aided Design Integr. Circuits Syst.*, vol. 38, no. 11, pp. 2086–2098, Nov. 2019.

[19] F. M. Tesche, "On the use of the Hilbert transform for processing measured CW data," *IEEE Trans. Electromagn. Compat.*, vol. 34, no. 3, pp. 259–266, Aug. 1992.

[20] S. Sercu, C. Kocuba, and J. Nadolny, "Causality demystified," in *Proc. Designcon*, Santa Clara, CA, USA, Jan. 2015, pp. 1–25. Accessed: Sep. 12, 2020. [Online]. Available: http://suddendocs.samtec.com/notesandwhitepapers/14-th1paper_causalitydemystified.pdf

[21] S. Sercu and L. Martens, "A new algorithm for experimental circuit modeling of interconnection structures based on causality," *IEEE Trans. Compon., Packag., Manuf. Technol.*, vol. 19, no. 2, pp. 289–295, May 1996.

[22] S. Luo and Z. Chen, "Iterative methods for extracting causal time-domain parameters," *IEEE Microw. Theory Techn.*, vol. 53, no. 3, pp. 969–976, Mar. 2005.

[23] A. M. Nicolson, "Broad-band microwave transmission characteristics from a single measurement of the transient response," *IEEE Trans. Instrum. Meas.*, vol. 17, no. 4, pp. 395–402, Dec. 1968.

[24] A. M. Nicolson and G. F. Ross, "Measurement of the intrinsic properties of materials by time-domain techniques," *IEEE Trans. Instrum. Meas.*, vol. 19, no. 4, pp. 377–382, Nov. 1970.

[25] R. Papazyan and R. Eriksson, "Calibration for time domain propagation constant measurements on power cables," *IEEE Trans. Instrum. Meas.*, vol. 52, no. 2, pp. 415–418, Apr. 2003.

[26] H. W. Loeb and P. J. Ward, "The use of time-domain techniques for microwave transistor S-parameter measurements," *IEEE Trans. Instrum. Meas.*, vol. 26, no. 4, pp. 383–388, Dec. 1977.

[27] A. V. Oppenheim and R. W. Schafer, *Discrete-Time Signal Processing* (Signal Processing Series). Upper Saddle River, NJ, USA: Prentice-Hall, 1999.

[28] W. Siebert, *Circuit Signal and Systems*. Cambridge, MA, USA: MIT Press, 1986.

[29] B. Gustavsen and A. Semlyen, "Rational approximation of frequency domain responses by vector fitting," *IEEE Trans. Power Del.*, vol. 14, no. 3, pp. 1052–1061, Jul. 1999.

[30] S. Grivet-Talocia, "Package macromodeling via time-domain vector fitting," *IEEE Microw. Wireless Compon. Lett.*, vol. 13, no. 11, pp. 472–474, Nov. 2003.

[31] T. Dhaene and D. Deschrijver, "Stable parametric macromodeling using a recursive implementation of the vector fitting algorithm," *IEEE Microw. Wireless Compon. Lett.*, vol. 19, no. 2, pp. 59–61, Feb. 2009.

[32] O. Salazar Celis, A. Cuyt, D. Deschrijver, D. V. Ginste, T. Dhaene, and L. Knockaert, "Macromodeling of high-speed interconnects by positive interpolation of vertical segments," in *Applied Mathematical Modelling*, vol. 37, no. 7, pp. 4874–4882, 2013.

[33] D. Deschrijver and T. Dhaene, "Rational fitting of S-parameter frequency samples with maximum absolute error control," *IEEE Microw. Wireless Compon. Lett.*, vol. 20, no. 5, pp. 247–249, May 2010.

[34] G. Antonini, "SPICE equivalent circuits of frequency-domain responses," *IEEE Trans. Electromagn. Compat.*, vol. 45, no. 3, pp. 502–512, Aug. 2003.

[35] S. Lalgudi, "On checking causality of tabulated S-parameters," *IEEE Trans. Compon., Packag., Manuf. Technol.*, vol. 3, no. 7, pp. 1204–1217, Jul. 2013.

[36] R. Zeng and J. Sinsky, "Modified rational function modeling technique for high speed circuits," in *IEEE MTT-S Int. Microw. Symp. Dig.*, 2006, pp. 1951–1954.

[37] G. B. Folland and A. Sitaram, "The uncertainty principle: A mathematical survey," *J. Fourier Anal. Appl.*, vol. 3, no. 3, pp. 207–238, May 1997.

[38] H. M. Nussenzveig, *Causality and Dispersion Relations*. New York, NY, USA: Academic, 1972.

[39] B.P. Lathi and R. Green, *Linear Systems and Signals*, 4th ed. Oxford, U.K.: Oxford Press, 2005.

[40] M. Tsiklauri, M. Zvonkin, J. Fan, J. Drewniak, Q. B. Chen, and A. Razmadze, "Causality and delay and physics in real systems," in *Proc. IEEE Int. Symp. Electromagn. Compat. (EMC)*, Raleigh, NC, USA, Aug. 2014, pp. 961–966.

[41] P. J. Pupalaikis, "The relationship between discrete-frequency S-parameters and continuous-frequency responses," in *Proc. Designcon*, Santa Clara, CA, USA, Feb. 2012, pp. 1–28.

[42] "Time domain analysis using a network analyzer," Keysight Technol., Santa Rosa, CA, USA, Appl. Note, Accessed: Sep. 12, 2020. [Online]. Available: https://www.keysight.com/us/en/assets/7018-01451/application-notes/5989-5723.pdf

[43] O. Ostwald, "Group and phase delay measurements with vector network analyzer ZVR," Rhode & Schwarz, Munich, Germany, Appl. Note 1EZ35_1E, Jul. 1997.

[44] G. Chaudhary, H. Choi, Y. Joeng, J. Lim, and C. D. Kim, "Design of group delay time controller based on a reflective parallel resonator," *ETRI J.*, vol. 34, no. 2, pp. 210–215, Apr. 2012.

[45] G. Strang and T. Nguyen, *Wavelets and Filter Banks Hardcover*, 2nd ed. Wellesley, MA, USA: Wellesley-Cambridge Press, Oct. 1996.

[46] M. Vetterli and J. Kovacevic, *Wavelets and Subband Coding* (Signal Processing Series). Upper Saddle River, NJ, USA: Prentice-Hall, Apr. 1995.

[47] R. J. Schilling and S. L. Harris, *Fundamentals of Digital Signal Processing Using MATLAB*, 2nd ed. Boston, MA, USA: Cengage, 2011.

[48] Y.-J. Shin *et al.*, "Application of time-frequency domain reflectometry for detection and localization of a fault on a coaxial cable," *IEEE Trans. Instrum. Meas.*, vol. 54, no. 6, pp. 2493–2500, Dec. 2005.

[49] S. Sercu, "Causality problems related to numerical modeling of interconnects and connectors," presented at the 9th Signal Integrity Symp., Harrisburg, PA, USA, Apr. 2015.

Aldo Morales (Senior Member, IEEE) was born in Tacna, Peru. He received the B.S. degree (Hons.) in electronic engineering from Northern University (now the University of Tarapaca), Arica, Chile, in 1978, and the M.Sc. and Ph.D. degrees in electrical and computer engineering from the University of Buffalo, The State University of New York at Buffalo, Buffalo, NY, USA, in 1986 and 1990, respectively.

He is currently a Professor of electrical engineering with Penn State Harrisburg, Middletown, PA, USA. He was the PI for a three-year Ben Franklin Technology Partners Grant that established the Center of Excellence in Signal Integrity at Penn State Harrisburg.

Dr. Morales was a coauthor for the Best Poster Paper Award at the IEEE International Conference on Consumer Electronics 2007, Las Vegas, NV, USA, for the article, Transmitter Pre-Emphasis and Adaptive Receiver Equalization for Duobinary Signaling in Backplane Channels. In addition, he was honored with the Best Paper Award at the IEEE Asia Pacific Conference on Circuits and Systems, Seoul, South Korea, in 1996, for the article, Basis Matrix Representation of Morphological Filters with N-Dimensional Structuring Elements. He was a PI for a $440K MRI NSF Grant and the DesignCon 13 Best paper Finalist. He was a PI for a Volvo grant.

Sedig S. Agili (Senior Member, IEEE) received the B.S., M.S., and Ph.D. degrees in electrical and computer engineering from Marquette University, Milwaukee, WI, USA, in 1986, 1989, and 1996, respectively.

Upon receiving his Ph.D. degree, he joined the faculty at Marquette University. In fall 2001, he joined the Electrical Engineering and Electrical Engineering Technology Programs at Penn State Harrisburg, Middletown, PA, USA, where he is currently a Professor, researching and teaching electronic communications, fiber optic communications, fiber optic sensors, and signal integrity of high-speed interconnects. He is the Co-Director of The Center of Excellence in Signal Integrity, Penn State Harrisburg. He has authored numerous articles that have been published in journals and conference proceedings.

Dr. Agili is also a Senior Member of the American Society for Engineering Education and a member of Sigma Xi. He was honored by the IEEE with the Best Poster Paper Award at the IEEE International Conference on Consumer Electronics 2007, Las Vegas, NV, USA, for the article Transmitter Pre-Emphasis and Adaptive Receiver Equalization for Duobinary Signaling in Backplane Channels. He received the 2010 Technical Achievement Award from the Central Pennsylvania Engineers Week Council. He was a Co-PI of a $440K MRI NSF Grant and the DesignCon 13 Best paper Finalist. He was a Co-PI of a Volvo industrial grant.

Taoufik Meklachi received the M.Sc. and Ph.D. degrees in applied mathematics from the University of Houston, Houston, TX, USA, in 2010 and 2014, respectively.

He has a Maitrise University of Hassan II Mohammedia 2002. Prior to joining Penn State Harrisburg, Middletown, PA, USA, he was an Assistant Visiting Professor with Drexel University, Philadelphia, PA, and a Post-Doctoral Research Associate with the University of Houston, where he worked on scattering theory and optics. His research interests are in mathematical physics, cloaking, optics, and inverse problems.

Dr. Meklachi is also a member of Society for Industrial and Applied Mathematics (SIAM), Philadelphia, PA.